Mobility of G proteins is heterogeneous and polarized during chemotaxis

Hemert, F. van; Lazova, M.; Snaar-Jagalska, B.E.; Schmidt, T.

Mobility of G proteins is heterogeneous and polarized during chemotaxis

Freek van Hemert[1,*], Milena D. Lazova[2,*], B. Ewa Snaar-Jagaska[2] and Thomas Schmidt[1,‡]

[1]Leiden Institute of Physics and [2]Leiden Institute of Biology, Leiden University, Niels Bohrweg 2, 2333 CA Leiden, The Netherlands

*These authors contributed equally to this work

‡Author for correspondence (schmidt@physics.leidenuniv.nl)

Accepted 24 May 2010
Journal of Cell Science 123, 2922-2930

doi:10.1242/jcs.063990

Summary

The interaction of G-protein-coupled receptors with G proteins is a key event in transmembrane signal transduction that leads to vital decision-making by the cell. Here, we applied single-molecule epifluorescence microscopy to study the mobility of both the Gβγ and the Gα2 subunits of the G protein heterotrimer in comparison with the cAMP receptor responsible for chemotactic signaling in *Dictyostelium discoideum*. Our experimental results suggest that ~30% of the G protein heterotrimers exist in receptor-precoupled complexes. Upon stimulation in a chemotactic gradient, this complex dissociates, subsequently leading to a linear diffusion and collision amplification of the external signal. We further found that Gβγ was partially immobilized and confined in an agonist-, F-actin- and Gα2-dependent fashion. This led to the hypothesis that functional nanometric domains exist in the plasma membrane, which locally restrict the activation signal, and in turn, lead to faithful and efficient chemotactic signaling.

Key words: Directional sensing, G protein signaling, G-protein-coupled receptor, Single-molecule biophysics

Introduction

G-protein-mediated signaling is a widely used mechanism for transmembrane signal transduction. It entails a seven-transmembrane receptor, the G-protein-coupled receptor (GPCR), and a heterotrimeric G protein consisting of a Gα and a heterodimeric Gβγ subunit. Compared with other transmembrane signaling systems, the complex, modular mechanics of G-protein-linked signaling allows for divergence, convergence and regulation to take place at the level of the GPCR–G protein complex by modulation of their interaction (Wettschureck and Offermanns, 2005). Mammalian genomes generally encode more than 1000 GPCRs, the majority of which do not have a known ligand. Although the atomic structure of three GPCRs has been resolved (Palczewski et al., 2000; Rasmussen et al., 2007; Jaakola et al., 2008), a mechanism for how ligand induced conformational changes lead to G protein activation is still unknown. Even the simple question of whether GPCRs and G proteins can exist together in a stable complex or interact dynamically has been solved for only one system (Nobles et al., 2005). In the dogmatic view, the ligand-based activation of the GPCR promotes the exchange of guanosine diphosphate (GDP) for guanosine triphosphate (GTP) in the Gα subunit, which subsequently dissociates from the complex, allowing both Gα and Gβγ to engage in downstream signaling. Hydrolysis of GTP to GDP in the Gα subunit, either autocatalytically or by effector proteins, leads to reassociation of the GPCR–Gαβγ complex.

An intriguing system in which GPCR signaling leads to a dramatic change in cellular behavior is that of eukaryotic chemotaxis. Chemotaxis controls the developmental cycle in the social amoeba *Dictyostelium discoideum*. Generally, chemotaxis is interpreted as a three-stage process starting with gradient sensing, followed by cellular polarization and ultimately results in directional movement. *D. discoideum* cells secrete cyclic adenosine monophosphate (cAMP), which acts as a chemoattractant leading to cell aggregation. Aggregation is achieved by a chemotactic process initiated by activation of the cAMP receptor 1 (cAR1), which in turn activates a G protein heterotrimer, consisting of a Gα2 and a Gβγ subunit (Kimmel and Parent, 2003). Sequencing of the *D. discoideum* genome showed that there is a single Gβ and a single Gγ subunit type in *D. discoideum* (Lilly et al., 1993; Zhang et al., 2001). Consequently, the Gβγ heterodimer participates in all GPCR-triggered responses. Receptor-mediated activation of heterotrimeric G protein complexes was visualized in *D. discoideum* using fluorescence resonance energy transfer (FRET) between the Gα2 and Gβ subunits, fused to cyan and yellow fluorescent proteins, respectively (Janetopoulos et al., 2001). These FRET experiments demonstrated that G protein heterotrimers are stable in the absence of agonist and rapidly dissociate upon addition of cAMP. Recently, the FRET experiments were complemented with fluorescence recovery after photobleaching (FRAP) data. A new model for G protein signaling was suggested in which the Gα2 increases the time it spends on the membrane or in a cAR1-bound state and the activated Gβγ subunit to dissociate into the cytosol. Both processes will lead to a cycling of the G protein heterotrimer between the membrane-bound and a free cytosolic state (Elzie et al., 2009).

Although many molecular details of the pathways are known, a direct connection between gradient sensing and the movement machinery is still to be determined. There are several pathways currently known to act in parallel downstream of G protein activation that mediate the final chemotactic response. The most thoroughly studied pathway involves phosphoinositide 3-kinase (PI3K) and its antagonist, a phosphoinositide 3-phosphatase (PTEN). The coordinated action of both leads to local accumulation of phosphatidylinositol (3,4,5)-trisphosphate [PtdIns(3,4,5)P_3] at the leading edge of the crawling cells (Iijima and Devreotes, 2002; Funamoto et al., 2002). Recently, additional signaling pathways have been found to act in parallel: the phospholipase A2 (PLA2) (Chen et al., 2007), the soluble guanylyl cyclase (sGC) (Veltman

Journal of Cell Science

et al., 2006), and the TorC2 (Kamimura et al., 2008) pathways all cooperate, presumably to achieve higher chemotactic efficiencies (Veltman et al., 2008).

In cells placed in a gradient of cAMP, the pathways downstream of G protein signaling trigger actin polymerization selectively in the cell leading edge, whereas actin polymerization occurs globally upon uniform cAMP stimulation (Chen et al., 2003). Unlike the highly polarized localization in actin polymerization and the preceding highly polar translocation of a variety of intracellular signaling molecules such as PtdIns(3,4,5)P_3 and PtdIns(4,5)P_2, receptor localization is fully homogeneous. The Gβγ subunit of the G protein is localized in a shallow anterior–posterior gradient, at a level of polarization that is impossible to restrict signaling to the leading edge (Jin et al., 2000). Recent studies (de Keijzer et al., 2008) revealed, however, a spatially restricted increase of receptor mobility in the leading edge of *D. discoideum* cells when exposed to a stable cAMP gradient. Those data suggested an asymmetry in the activation level of the receptor–G-protein pathway with a predicted linear amplification of the local activation level of the G proteins.

Here, we set out to address this prediction. We analyzed Gα2 and Gβγ mobility in the absence of agonist, upon uniform cAMP stimulation, and in a cAMP gradient using single-molecule epifluorescence microscopy (Schmidt et al., 1996). We found that Gα2 and Gβγ occur as a smaller (~30%) receptor-precoupled fraction, and a larger (~70%) receptor-uncoupled fraction. Upon global stimulation with cAMP, the receptor-coupled fraction disappeared. In terms of the receptor, those occupation numbers correspond to about 50% of all available receptors. The activated Gβγ molecules immobilize in an F-actin-dependent manner. Concurrently, the formation of F-actin-dependent domains of ~600 nm was observed. Strikingly, the dramatic changes in mobility were restricted to the leading edge of chemotaxing cells. We propose that Gβγ immobilization is caused by its incorporation into a larger signaling complex, a signalosome, for which F-actin functions as a scaffold. Such a mechanism would lead to stabilization of pseudopods and the formation of a persistent leading edge by means of a direct F-actin–G-protein feedback loop.

Results

Heterogeneity in the mobility of Gα2-YFP and Gβ-YFP in the absence of agonist

D. discoideum cells were transformed stably with Gα2-YFP or Gβ-YFP constructs to analyze the mobility of individual Gα2 and Gβγ molecules, respectively. The fluorescent fusion proteins were shown to be functional because they rescued the developmental and chemotactic defects of *gα2*$^-$ and *gβ*$^-$ cells. In contrast to *gα2*$^-$ and *gβ*$^-$ cells, which are both fully deficient in cAMP-induced responses, the Gα2-YFP *gα2*$^-$ and Gβ-YFP *gβ*$^-$ transformants faithfully crawl towards a cAMP source and rescue the developmental cycle started upon starvation (Jin et al., 2000; Janetopoulos et al., 2001).

Single-molecule microscopy, a combination of regular wide-field microscopy with laser excitation and ultra-sensitive CCD camera detection (Schmidt et al., 1996), was used to observe the diffusion of Gα2-YFP and Gβ-YFP on the apical cellular membrane of *D. discoideum*. Measurements on the apical membrane eliminate any potential influence of the substrate surface on mobility. Fluorescence images were taken consecutively for up to 500 images per sequence at an imaging rate of 20 Hz. Diffraction-limited fluorescent signals with signal strengths comparable with that reported for individual monomeric YFP molecules (Harms et al., 2001) were observed and followed over time (Fig. 1B,C). Given the signal-to-noise ratio achieved, the position of each molecule was determined to an accuracy of ~40 nm. Statistical significance of all results was assured by the analysis of more than 40 cells for each experimental condition. In total, our analysis is based on 1×10^4 to 4×10^4 observed molecules per condition.

Particle image correlation spectroscopy (PICS) (Semrau and Schmidt, 2007) was subsequently applied to construct the cumulative probability (cumulative density function, c.d.f.) of the

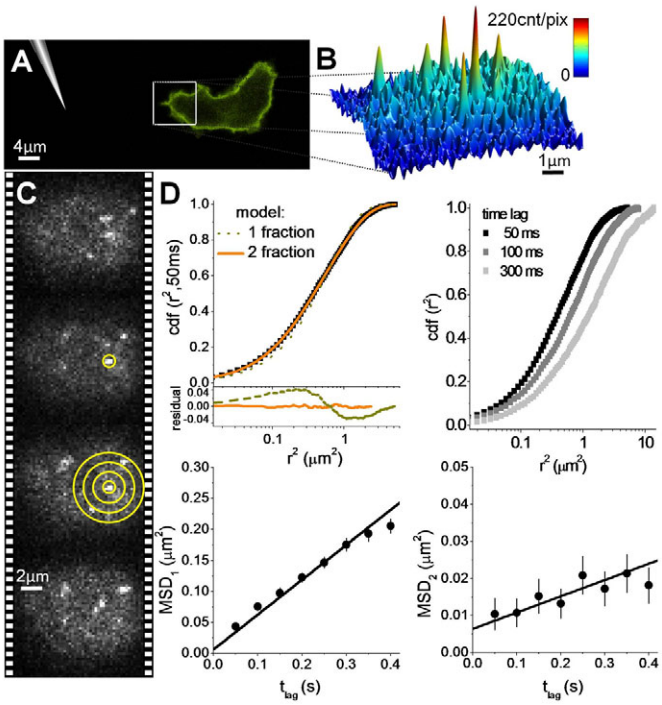

Fig. 1. Experimental set-up. (**A**) A micropipette containing 10 μM cAMP is used to create a stable concentration gradient around its opening. *D. discoideum* cells in the vicinity of the pipette polarize within minutes and move up the cAMP concentration gradient. The anterior and posterior of a cell was defined as the part closest and farthest away from the pipette, respectively. (**B**) A 514 nm laser beam was focused on the apical cell membrane where signals originating from individual Gβ-YFP or Gα2-YFP proteins were observed with a signal-to-noise ratio of ~30. (**C**) The image stacks were scanned for single molecule signatures of which the positions were determined to an accuracy of ~40 nm by fitting to a 2D Gaussian profile. Using particle image correlation spectroscopy (PICS), the cumulative probability density as a function of jump distance (r^2, yellow circles) for each time lag (t_{lag}=50 mseconds between subsequent images) [$cdf(r^2,t_{lag})$] was constructed. (**D**) $cdf(r^2)$ at a time lag of 50 mseconds is fitted to a two-component model (Eq. 4, orange solid line) [one-component model is shown for comparison (Eq. 3, dark-yellow dashed line)]. This results in 2 MSDs and a size denominator for both fractions, α and 1-α (top left). The same process is repeated for multiple time lags (up to eight), as expected the data shifts with time lag towards higher squared displacements (top right). The mean-squared displacements are plotted versus time lag for the slow fraction (bottom left) and the fast fraction (bottom right) of Gβ-YFP in naive wt cells. The free-diffusion model (Eq. 1) yielded diffusion constants of D_1=0.15±0.01 μm^2/second and D_2=0.011±0.001 μm^2/second. The offset at zero time lag, s_0, in C and D is given by the limited positional accuracy, $s_0=4\sigma_0^2$=0.0064 μm^2. The mobility of the slow fraction is equivalent to that of the cAMP receptor D_{cAR}=0.012 μm^2/second (data not shown). Error bars indicate s.e. obtained from ten bootstrap runs of the fitting routine.

squared displacements for time-lags of 0.05–0.4 seconds (Fig. 1C,D). To our surprise, it became obvious for all c.d.f. values that G protein mobility was not homogeneous and was best described by a two-fraction model (Fig. 1D), which, after fitting, yielded a fraction size and two mean-squared displacements per time lag (see the Materials and Methods). The result of a final analysis is shown in Fig. 1D for the fast and slow fraction of Gβ-YFP in non-stimulated aggregation-competent cells, respectively (see Fig. 3 for results on Gα2-YFP). For both fractions, the mean-squared displacement, MSD, increased linearly with time lag, indicative of free Brownian motion of the proteins within the membrane characterized by diffusion constant D,

$$MSD(t_{lag}) = 4Dt_{lag} + s_0 , \quad (1)$$

where the offset, s_0, accounts for the limited positional accuracy, σ, in the experiment ($s_0=4\sigma^2=0.0064$ μm^2 with σ=40 nm). Because the Gγ subunit has been shown to be essential for the membrane localization of Gβ (Zhang et al., 2001) we assume, in what follows, that Gβγ is in heterodimeric form and all information obtained for Gβ reflects in an identical manner the behavior of Gγ. For Gβγ-YFP in unstimulated cells, the fast fraction was characterized by a diffusion constant D_1=0.15±0.01 μm^2/second, and the slow fraction, consisting of 32±3% of all molecules, was characterized by D_2=0.011±0.001 μm^2/second. For the membrane-bound Gα2-YFP in unstimulated cells the respective diffusion constants of the fast and the slow fraction were D_1=0.14±0.01 μm^2/second and D_2=0.015±0.001 μm^2/second, with the slow fraction constituting 32±4% of the total pool of molecules (Fig. 3). Identical results for the mobility and fraction size of Gα2 and Gβγ were obtained in *gα2*$^-$ and *gβ*$^-$ cells that expressed Gα2-YFP and Gβ-YFP, respectively, at endogenous levels (supplementary material Fig. S1). The latter findings proved that the predominant fast fraction was not an artifact caused by the overexpression of the constructs in a wild-type background.

Mobility suggests the existence of a receptor–G-protein precoupled complex in the absence of agonist

The strong similarity of the diffusion constants of both fractions for Gα2 and Gβγ further suggests that all membrane-bound G proteins in unstimulated cells were Gα2βγ heterotrimers. It is tempting to associate the slow mobility fractions of Gα2 and Gβγ to a receptor–G-protein precoupled complex. The G protein diffusion constants (D_2=0.015 μm^2/second for Gα2 and D_2=0.011 μm^2/second for Gβγ) were similar to that found for the fast fraction of the receptor cAR1 [MSD(44 mseconds)=0.034 μm^2 (de Keijzer et al., 2008); D=0.015 μm^2/second, our unpublished results). However, the diffusion constants of the fast fractions of the G protein subunits in unstimulated, aggregation-competent cells were one order of magnitude higher than that found for cAR1, demonstrating that the fast fraction cannot be associated with a receptor-precoupled complex.

The association of the slow G protein fractions with a receptor–G-protein precoupled complex was further supported by the analysis of Gβ-YFP mobility in *car1*$^-$ and in *gα2*$^-$ cells (Fig. 2). Both, Gβ-YFP *car1*$^-$ and Gβ-YFP *gα2*$^-$ cells were fully deficient in chemotactic signaling and unable to aggregate. For both cell types, mobility was best described by a two-fraction model, with decreased slow fraction size of 18±3% and 27±4% for Gβ-YFP *car1*$^-$ and Gβ-YFP *gα2*$^-$, respectively (Fig. 2A). In addition, the diffusion constants of the slow fraction of Gβ-YFP in both knockout cell types was found to be D_2=0.020±0.001 μm^2/second in *gα2*$^-$ and D_2=0.023±0.001 μm^2/second in *car1*$^-$, respectively (Fig. 2B, left), higher than the diffusion constants in wild-type cells, and in particular the diffusion constant of cAR1. In comparison, the mobility of the fast fractions, D_1=0.16±0.01 μm^2/second in *gα2*$^-$ and D_1=0.19±0.01 μm^2/second in *car1*$^-$, were unchanged compared with wild-type cells (Fig. 2C, left). Within levels of experimental uncertainty, Gα2 mobility was unchanged in *car1*$^-$ and *gβ*$^-$ cells (Fig. 3B,C, left).

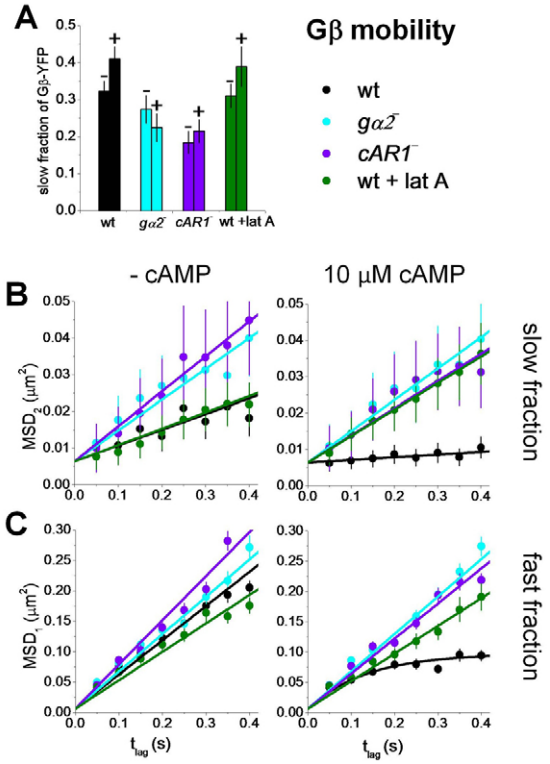

Fig. 2. Mobility of Gβ-YFP upon stimulation. (**A**) Size of the slow fraction for Gβ-YFP in wt (black) and *gα2*$^-$ (light blue), *car1*$^-$ (violet) and wt cells treated with 0.5 μM lat A (green), before and after global stimulation with 10 μM cAMP (indicated by – and +, respectively). The slowly diffusing population of Gβ-YFP in wt cells increased after cAMP stimulation. The slow fractions of Gβ-YFP in *gα2*$^-$ and *car1*$^-$ were smaller and did not change significantly upon cAMP addition. In latA-treated cells, the slow fraction was the same when compared with untreated cells. After stimulation, however, there was an increase similar to that found for cells with intact actin cytoskeleton. (**B**) MSD$_2$ versus time-lag plot of the slow fraction of Gβ-YFP in wt (black), *gα2*$^-$ (light blue), *car1*$^-$ (violet), and wt cells after treatment with 0.5 μM latA (green) before (left) and after (right) stimulation with 10 μM cAMP. In wt cells, the slow fraction was fully immobilized after cAMP stimulation. Gβ-YFP in *gα2*$^-$ and *car1*$^-$ cells was diffusing nearly twice as fast as Gβ-YFP in wt cells. In the knockout strains, cAMP addition did not influence the diffusion constants, suggesting that immobilization of the slow population of Gβ-YFP in wt cells was due to signaling events. LatA-treated wt cells did not show any immobilization, suggesting that immobilization is caused by interaction of the Gβ subunit with F-actin structures. (**C**) MSD$_1$ versus time lag of the fast fraction of Gβ-YFP in wt (black), *gα2*$^-$ (light blue), *car1*$^-$ (violet), and wt cells treated with 0.5 μM lat A (green) before (left) and after (right) stimulation with 10 μM cAMP. The diffusion behavior of Gβ-YFP in wt cells changed from free (Eq. 1) to confined (Eq. 2) upon cAMP stimulation. This was not observed in latA-treated, *gα2*$^-$ and *car1*$^-$ cells, where G protein signaling was impaired. All values are means ± s.e. obtained from ten bootstrap runs of the fitting routine.

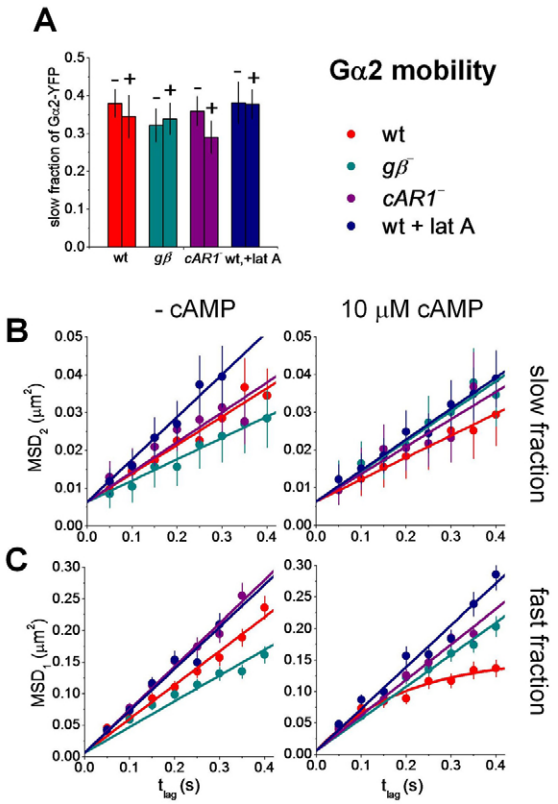

Fig. 3. Mobility of Gα2-YFP upon stimulation. (**A**) Size of the slow fraction of Gα2-YFP in wt (red), gβ⁻ (cyan), *car1*⁻ (purple), and cells treated with 0.5 µM latA (blue), before (–) and after (+) global stimulation with 10 µM cAMP. (**B**) MSD_2 versus time lag of the slow fraction of Gα2-YFP in wt (red), *gα2*⁻ (cyan), *car1*⁻ (purple), and cells treated with 0.5 µM latA (blue) before (left) and after (right) uniform stimulation with 10 µM cAMP. The diffusion of the slow fraction of Gα2-YFP was not influenced by stimulation with cAMP, knockout of gβ, or disruption of the F-actin cytoskeleton. (**C**) MSD_1 versus time lag of the fast fraction of Gα2-YFP in wt (red), gβ⁻ (cyan), *car1*⁻ (purple), and cells treated with 0.5 µM latA (blue) before (left) and after (right) uniform stimulation with 10 µM cAMP. The diffusion behavior of Gα2-YFP in wt changed from free (Eq. 1) to confined (Eq. 2) upon cAMP stimulation. This was not observed for latA-treated, gβ⁻ or *car1*⁻ cells. All values are means ± s.e. obtained from ten bootstrap runs of the fitting routine.

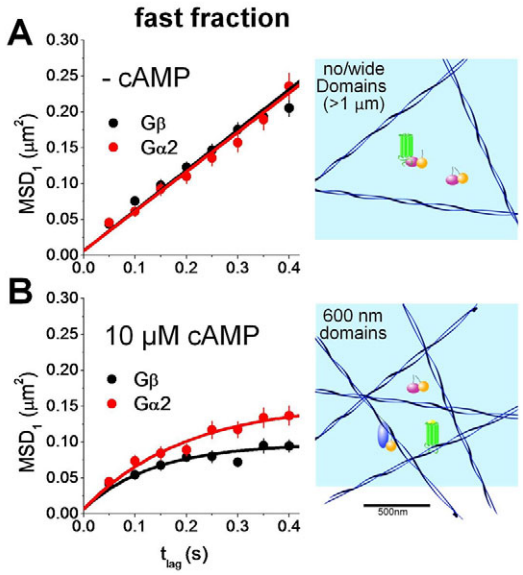

Fig. 4. Comparison of the mobility of the fast fractions of Gβ-YFP and Gα2-YFP. The behavior of the fast Gβ-YFP (black) and Gα2-YFP (red) on the apical membrane of wt *D. discoideum* (**A**) before, and (**B**) after uniform stimulation with 10 µM cAMP changes from free to confined diffusion, respectively. The formed domains have an average side length of 600 nm. Error bars represent s.e. obtained from ten bootstrap runs of the fitting routine.

Additional support for our hypothesis on association of the slow fraction with a receptor–G-protein precoupled complex was obtained from the estimated expression levels of all components in wild-type and knockout cells. We used the membrane-localized fluorescence signal to estimate the density of Gβ-YFP and Gα2-YFP (see the Materials and Methods). Approximately 7.7×10^4 Gβ-YFP were expressed, which is at the lower end of the expression level of reported endogenous Gβγ molecules of 8×10^4–40×10^4 molecules (Jin et al., 2000). It was reported earlier that 4×10^4 receptors were expressed in wild-type and in transformed cells (Van Haastert et al., 1996; de Keijzer et al., 2008), the active fraction of which, 2×10^4 (~50% of 4×10^4) (de Keijzer et al., 2008) corresponds very well to the number of slow Gβγ molecules, 2.5×10^4 (~32% of 7.7×10^4).

A fraction of Gβ-YFP becomes immobilized upon cAMP-induced receptor activation

To study the effect of cAMP-induced activation on Gα2 and Gβγ mobility, cells were uniformly stimulated with 10 µM cAMP. Single-molecule data were taken between 1 and 20 minutes after addition of cAMP (see the Materials and Methods). A redistribution of the fraction sizes and mobilities was observed. The slow fraction of Gβ-YFP increased to 41±3% upon stimulation (Fig. 2A), and became immobile ($D_2\leq0.001$ µm²/second; Fig. 2B, right).

Neither immobilization nor change in fraction size was observed for Gα2-YFP (Fig. 3A,B). Because Gα2 cycles rapidly between the membrane and the cytosol upon stimulation of cAR1 (Elzie et al., 2009), this latter finding suggests that a receptor–Gα2 complex is formed before the full receptor–G-protein heterotrimer complex.

The increase of the Gβ-YFP slow fraction and concomitant immobilization was not observed in Gβ-YFP *car1*⁻ and Gβ-YFP *gα2*⁻ cells, where the slow fraction was 22±4% and 21±3% after stimulation, respectively (Fig. 2A,B, right). This remaining slow fraction might be bound to other Gα subunits that are related to signaling via other G protein coupled receptors. Whereas the result on Gβ-YFP *car1*⁻ was predicted, the lack of Gβ-YFP response in Gβ-YFP *gα2*⁻ cells supports the notion that coupling to and activation by cAR1 requires Gα2. These observations together were taken as further support for the hypothesis that the slow Gα2-YFP and Gβ-YFP population reflected a receptor–G-protein precoupled complex, which dissociates upon ligand binding and receptor activation.

cAMP stimulation induces confined diffusion of fast Gα2-YFP and Gβ-YFP fractions into 600 nm membrane domains

Upon global cAMP stimulation, the fast fractions of both Gα2-YFP and Gβ-YFP changed their behavior from free diffusion (Eq. 1) to confined diffusion (Fig. 4, Eq. 2). Confined diffusion is a process in which a molecule is free to diffuse in a restricted domain

surrounded by impermeable fences. The corresponding relation between MSD and time lag is:

$$MSD(t_{lag}) = \frac{L^2}{3}\left(1 - \exp\left(\frac{-12\,D_{init}t_{lag}}{L^2}\right)\right) + s_0\ , \qquad (2)$$

where D_{init} is the initial diffusion coefficient for small time lags, and L represents the side length of a square domain (Kusumi et al., 1993). From Fig. 4B, the domain size was determined to be 600±100 nm for both Gα2-YFP and Gβ-YFP, and the initial diffusion constants $D_{init,1}$=0.19±0.02 and $D_{init,1}$=0.16±0.02 μm^2/second for the two constructs, respectively.

cAMP-induced membrane domains and Gβ-YFP immobilization are F-actin dependent

To determine whether there is a relation between actin polymerization, the 600 nm membrane domains, and the cAMP-induced immobilization of the Gβγ slow fraction, aggregation-competent Gβ-YFP wt cells were incubated with 0.5 μM latrunculin A (latA) for 10 minutes. The diffusion behavior of Gα2-YFP and Gβ-YFP was unchanged after latA treatment in unstimulated cells (Fig. 2B,C, left; Fig. 3B,C, left). However, upon global stimulation with 10 μM cAMP, a significant change in diffusion behavior was observed. The slow fraction size of Gβ-YFP increased slightly to 39±5%, and the immobilization seen for untreated cells disappeared (D_2=0.016±0.001 μm^2/second; Fig. 2B, right). Furthermore, the confinement observed in the fast fractions of Gα2-YFP and Gβ-YFP vanished and both constructs diffused freely with D_1=0.15±0.01 μm^2/second (Fig. 2C, right; Fig. 3C). These results led us to conclude that the membrane domains observed were F-actin dependent, and that immobilization of Gβ-YFP required either a direct or an indirect interaction of Gβ-YFP with the F-actin meshwork. It should be noted, however, that the increase of the slow fraction upon global cAMP stimulation was undisturbed by latA. By contrast, the immobilization of the slow Gβ-YFP fraction was clearly regulated by F-actin and is presumably involved in maintaining cell polarity during chemotaxis.

The increase of the slow fraction and Gβγ immobilization occurs selectively in the leading edge of *D. discoideum* cells

Whether the increase of the slow fraction and immobilization of Gβ-YFP upon global stimulation with 10 μM cAMP reflects a differential G protein behavior in the chemotaxis process was subsequently tested in a micropipette assay. The opening of a micropipette, filled with 10 μM cAMP, was placed at a distance of 75 μm from the cells generating a shallow cAMP gradient of ~0.4 nM/μm at the cell position. After 1–3 minutes, cells became highly polarized and oriented towards the micropipette (Fig. 1A). The size of the slow fraction of Gβ-YFP differed significantly when comparing leading to trailing edge, which were found to be 38±4% and 23±3%, respectively (Fig. 5A). Strikingly we found that the diffusion constants of the slow fraction were different at the anterior compared with the posterior: at the anterior, the slow Gβ-YFP fraction was immobilized (D_2<0.001 μm^2/second; Fig. 5C, left) exactly as observed upon global stimulation, whereas at the posterior, the diffusion constant was comparable with that found for unstimulated cells (D_2=0.012±0.001 μm^2/second). We also found that the formation of the characteristic 600 nm domains was restricted to the anterior (Fig. 5B). All together, the behavior of Gβγ in the absence of agonist matches the behavior in the posterior, whereas Gβγ behavior at the anterior matches the situation observed after global agonist stimulation. Micropipette experiments on latA-treated cells confirmed that F-actin, in part, controls G protein mobility in an activation-dependent manner. As latA-pretreated cells did not evolve any morphological polarity, we defined the part nearest to the micropipette as the anterior. The posterior part of the cell was defined accordingly. The difference in slow fraction size between the anterior and the posterior cell regions was found to be the same as that found in polarized cells with intact cytoskeleton (Fig. 4A, right). This finding could have been

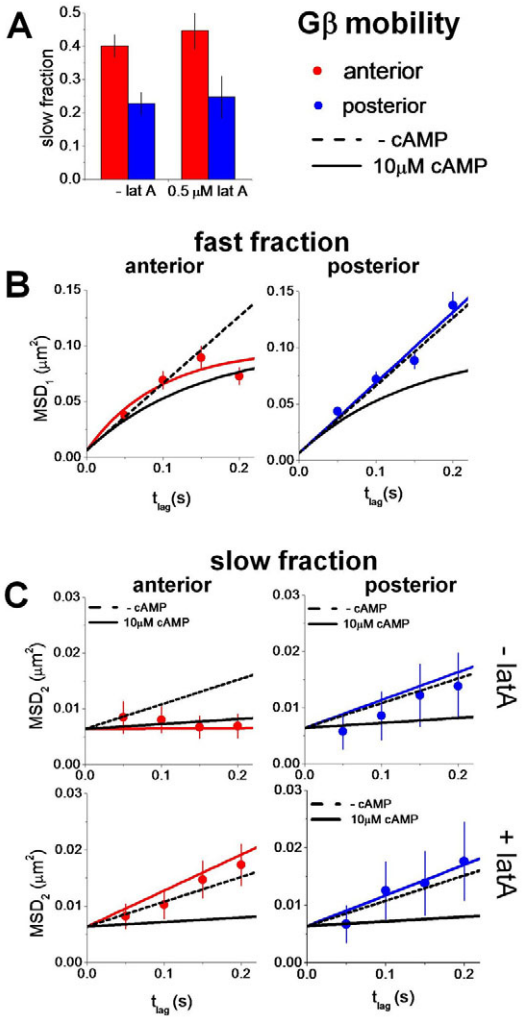

Fig. 5. Gβ-YFP mobility is highly polarized. The diffusion of Gβ-YFP in the anterior (red) and the posterior (blue) apical membrane of wt *D. discoideum* crawling in a shallow (0.4 nM/μm) cAMP gradient shows distinct differences. The black lines show the results obtained for cells before (dashed line; Fig. 1D, lower left and right) and after global stimulation with 10 μM cAMP (solid line, Fig. 1D, lower right). (**A**) Slow fraction size of Gβ-YFP in the leading (red) and trailing (blue) edge of wt cells (left) and cells treated with latA. (**B**) MSD_1 versus time lag for the fast fraction in the leading (red) and trailing edge (blue). Confinement was only observed for the fast fraction at the anterior upon stimulation with a cAMP gradient. (**C**) MSD versus time plot for the slow fraction in the leading (red) and trailing edge (blue) in wt cells (top) and cells treated with latA (bottom). In the wt cells, the slow fraction was immobilized in the front (D<0.001 μm^2/second). Immobilization was not observed in latA-treated cells. All values are means ± s.e. obtained from ten bootstrap runs of the fitting routine.

predicted given that gradient sensing is an actin-independent process. Similarly to the case of uniform cAMP stimulation, the immobilization of Gβ-YFP at the anterior, as well as the confined diffusion behavior of the fast fraction disappeared upon F-actin disruption.

cAMP-induced domain formation is independent of PI3K and PLA2

To investigate whether the observed cAMP-induced changes in the mobility of the Gβ subunits are the consequence of the activity of the PI3K pathway, we treated the cells with the PI3K inhibitor LY294002. At a concentration of 60 μM and incubation times of 15 minutes, PI3K activity is reduced by >95% (Chen et al., 2007). In the absence of agonist, the inhibitor did not influence the mobility of Gβ subunits. Uniform stimulation with 10 μM cAMP also resulted in diffusion parameters that were similar to the control situation of wild-type cells stimulated with cAMP. The fast fraction was confined, revealing the presence of ~600 nm domains (Fig. 6C). The slow fraction in LY294002-treated cells was significantly slowed (D_2=0.006±0.001 μm^2/second), but mobile (Fig. 6B). Similarly to the control experiments on global cAMP stimulation, the size of the slow fraction grew by 17% (Fig. 6A).

The observed results suggested that the F-actin-dependent domain formation was independent of PI3K activity. Although the PI3K–PTEN pathway is known to be important for ligand-induced actin polymerization, the latter finding is probably justified by the presence of parallel pathways. Therefore, in addition to LY294002, we also used the PLA2 inhibitor bromoenol lactone (BEL) at a saturating concentration of 5 μM (Chen et al., 2007). Cells were incubated with both inhibitors and subsequently stimulated with 10 μM cAMP. Treatment with both inhibitors did not result in any significant change in the mobility when compared with treatment with LY294002 alone (Fig. 6B). This result further proved the notion that additional pathways act in parallel to PI3K and PLA2 pathways and that they are sufficient for actin reorganization, albeit at a reduced efficient compared with when all pathways are active.

Discussion

The spatiotemporal behavior and interaction of activated GPCRs with G proteins constitutes a key event in chemotaxis. Using single-molecule epifluorescence microscopy we measured G protein diffusion in the absence and presence of agonist and in cells in an agonist gradient. By analysis of the mobility in various signaling states, we developed a mechanistic model of the early steps in chemotactic signaling (Fig. 7). In the inactive state (Fig. 7, top), G proteins at the membrane are in one of two fractions: a highly mobile Gα2βγ heterotrimer or a low-mobility receptor–Gα2βγ precoupled complex. The receptor–Gα2βγ complex, which accounts for 32% of the membrane-bound Gα2, 32% of the Gβγ, and 50% of the activatable receptor population, was identified by comparison of their mobility. Binding of the G protein to the receptor leads to a slow-down in its mobility by one order of magnitude. This latter finding is in line with recent FRAP and TIRFM experiments (Elzie et al., 2009) in which an increase in membrane-bound G protein fraction on receptor activation has been found and attributed to G-protein–receptor interaction. Given that fast cytosolic proteins (Potma et al., 2001) are not visible with our technique and only lead to an increased background signal, our results provide a detailed view on the membrane-bound fraction and the processes that have a role within the membrane.

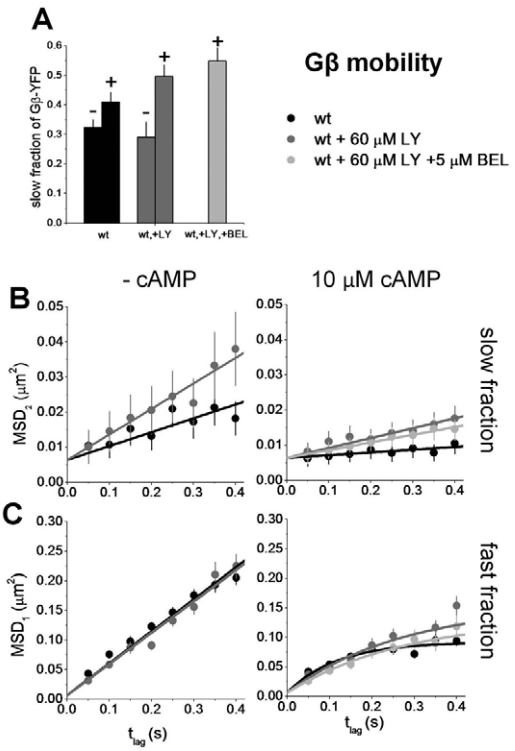

Fig. 6. Mobility of Gβ-YFP on inhibition of PI3K and PLA2. Diffusion of Gβ-YFP on the apical membrane of wt *D. discoideum* treated with the PtdIns(3,4,5)P_3 kinase inhibitor LY294002, and the PLA2 inhibitor bromoenol lactone (BEL). (**A**) Size of the slow fraction of Gβ-YFP before and after uniform stimulation with 10 μM cAMP in wt cells (black), cells treated with LY294002 (gray) and cells treated with both LY294002 and BEL (light gray). (**B**) MSD_2 versus time lag of the slow fraction of Gβ-YFP in wt cells (black), cells treated with LY204002 (gray), and cells treated with both LY294002 and BEL (light gray) before (left) and after (right) uniform stimulation with 10 μM cAMP. cAMP stimulation caused a dramatic slow down of the diffusion of the slow fraction in wt cells. This slow down was impaired after treatment with both inhibitors. (**C**) MSD_1 versus time plot of the fast fraction of Gβ-YFP in wt cells (black), cells treated with LY294002 (gray), and cells treated with both LY294002 and BEL (light gray) before (left) and after (right) uniform stimulation with 10 μM cAMP. Confinement upon cAMP stimulation was observed even in presence of both LY294002 and BEL. These findings suggest that a third parallel pathway, which was not inhibited [most likely the TorC2 pathway (Kamimura et al., 2008)], is acting in gradient sensing. All values are means ± s.e. obtained from ten bootstrap runs of the fitting routine.

Receptor activation by stimulation with cAMP (Fig. 7, bottom) disrupts the equilibrium between the Gα2βγ heterotrimer and the receptor–Gα2βγ precoupled complex by allowing the latter to form an activated receptor–Gα2βγ complex. This intermediate complex subsequently dissociates into a free activated receptor, and into free Gβγ and Gα2^{GTP} subunits. As argued by de Keijzer and colleagues (de Keijzer et al., 2008), the activated cAMP-receptor is able in turn to interact with and activate further Gα2βγ heterotrimers (68% of the initial Gβγ and the membrane-bound Gα2 population) (Fig. 7, bottom, red arrows), resulting in a local increase of G protein activation until cAMP dissociates from cAR1 at a rate of 0.4–1 second^{-1} (Janssens and Van Haastert, 1987). It was predicted earlier (de Keijzer et al., 2008) that such a local amplification step, governed by the simultaneous increase in

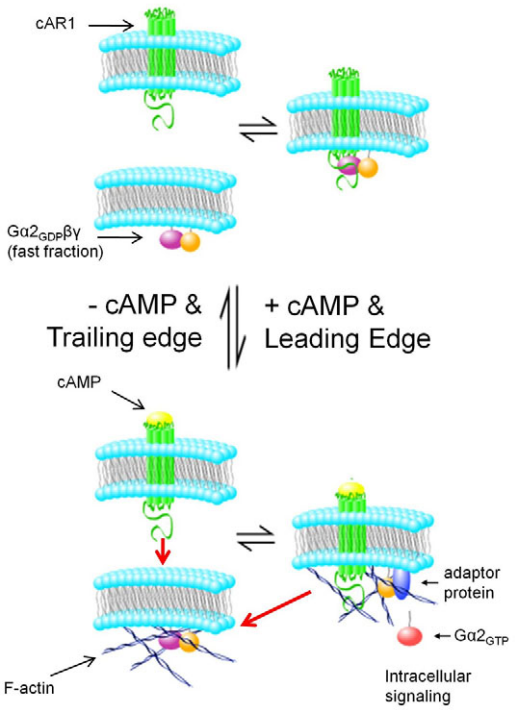

Fig. 7. Model describing the dynamic cAR1–G-protein interaction at the leading and trailing edge. Before cAMP stimulation (top) the G protein fast fraction is diffusing freely on the membrane with diffusion constant D=0.15 μm^2/second. The slow fraction (D=0.011 μm^2/second) exists as a complex, which is precoupled to cAR1. 30% of the G protein and about 60% of the receptor population exist in this fraction. Upon binding of cAMP to the receptor (bottom), the G protein heterotrimer is dissociated: the Gα2 subunit exchanges GDP for GTP and diffuses into the cytosol where it is free to activate downstream signaling molecules. The previously precoupled cAR1 fraction is engaged in catalytic activation of the large G protein heterotrimer pool (indicated by red arrows). The Gβγ heterodimeric subunit is immobilized by interaction with F-actin associated structures, which potentially serve to locally enhance chemotactic signaling. Tightening of membrane-associated F-actin restricts the diffusion of G proteins to ~600 nm domains.

receptor mobility, will lead to a final fivefold linear amplification of the external cAMP gradient to an intracellular gradient in active Gβγ proteins. The current experiments confirmed this prediction. Using the diffusion behavior of the G proteins as characterized here for the finite-element model described before (de Keijzer et al., 2008), we found that one cAR1 receptor activates 5–10 G proteins at gradient conditions that were experimentally realized.

In parallel to the increase in fraction size, we observed a slow-down of Gβγ mobility upon stimulation. Since measurements were performed within 20 minutes of stimulation, a time after which adaptive processes have been initiated (Devreotes and Steck, 1979; Wessels et al., 1989), we conclude that the immobilization is not transient, but persists as long as cells are stimulated. The observation confirms the previously observed dose-dependent steady-state loss of FRET, which was explained by the dissociation of the Gα2βγ complex into its subunits (Janetopoulos et al., 2001).

Following G protein activation and further downstream signaling, the actin cytoskeleton is reorganized (Franca-Koh et al., 2006). Reorganization leads to a tightening of membrane-associated F-actin, which is apparent in Gα2 and Gβγ mobility and shows confinement to F-actin-dependent domains of ~600 nm in size. At this point, it is still unclear whether F-actin is sufficient for Gβγ immobilization or whether associated proteins are needed to allow for the immobilization to occur. Inhibition of downstream PI3K (with 60 μM LY294002) and PLA2 (with 5 μM BEL), however, revealed that Gβγ slow-down was dependent on PI3K and PLA2 only to a certain degree. Complete immobilization, as in the control experiment, was not observed. This might indicate either immobilization of only a part of the Gβγ subunits, binding to less rigid F-actin fibers, or the fact that F-actin polymerizes only partially, as shown upon addition of any of these two inhibitors (Chen et al., 2007).

The formation of the 600 nm F-actin-dependent domains, by contrast, was undisturbed. The restriction of activated signaling molecules to a small part of the membrane by inhibiting them from moving across the cell leads to a suggestive biological role for F-actin-mediated confinement. Indeed, the leading edge of moving epidermal keratocytes isolated from fish has been described as a diffusion barrier, even for lipids (Weisswange et al., 2005).

Clustering of signaling components into a multicomponent signaling complex via a scaffold and/or anchoring proteins to the cytoskeleton was found for various signaling cascades (Pawson and Scott, 1997) and seems ubiquitous. After initial G protein activation and respective activation of downstream signaling, enhanced actin polymerization is observed at the front. Activated Gβγ subunits are constrained to actin-dependent scaffolds at the leading edge. This process, which spatially restricts Gβγ signaling, might in turn lead to a further enhancement of the related signaling cascade at the anterior of the cell in an F-actin-dependent positive-feedback loop. This process might facilitate chemotactic signaling by spatially restricting the activated signaling components in a larger protein complex: a signalosome. Our data show that, if domains are present before stimulation, they must have a side-length of L>1 μm (Fig. 1D, lower left). Upon stimulation, such domains shrink to L=600 nm (Fig. 1D, lower right). Assuming a homogeneous distribution of receptors and G proteins in the cell membrane (surface area=540 μm^2, see the Materials and Methods) before stimulation, we estimate that such domains on average contain 4×10^4 receptors per 540 μm$^2\times$(600 nm)^2=27 receptors, ~48 Gα2 subunits and ~ 52 Gβγ subunits. Experiments performed on F-actin-depleted cells have revealed that gradient sensing, the mere detection of the chemical gradient, was not impaired (Parent et al., 1998). Hence, the role of Gβγ immobilization is probably related to the stabilization of pseudopods and perhaps, at a later stage, to the development of an innate cell polarity as is observed after prolonged directional stimulation of *D. discoideum* (Franca-Koh et al., 2006).

A variety of studies have clearly demonstrated that gradient sensing is reflected as a remarkable relocation of signaling components shortly after application of the chemical gradient (Parent et al., 1998; Comer and Parent, 2002; Xu et al., 2005). PtdIns(3,4,5)P_3 and its related kinase (PI3K) are largely localized at the leading edge, whereas their related phosphatase (PTEN) is excluded from the anterior (Iijima and Devreotes, 2002). Despite extensive research, relocation of neither the receptor nor the G protein has ever been observed. Protein behavior and activation can be different at different locations owing to local variations in membrane curvature (Fischer et al., 2007), activated signaling cascades (Ueda et al., 2001) and the presence of signaling scaffolds (Pawson and Scott, 1997). Our experiments here show, as for the cAMP receptor, that cell polarization is reflected in a dynamic

property of the G proteins, namely their mobility, rather than in their localization. It is noteworthy that the polarized distribution of Gβγ mobility was found to be independent of the presence of F-actin: an identical distribution between fast (inactive) and slow (active) fractions was observed in cells treated with 0.5 μM latA. From the fact that the initial diffusion constant, in contrast to the MSD behavior over time, is equal across the cell body during chemotaxis, we conclude that the 3D membrane structure is not an important factor in the interpretation of the molecular mobilities. Together, we conclude that the increase in G protein activity is related to gradient sensing and not to processes responsible for subsequent pseudopod stabilization or amplification and persistent cell polarity.

We and other groups have shown before that polarization in chemotaxing *D. discoideum* cells is present at the level of the GPCR (Ueda et al., 2001; de Keijzer et al., 2008). Here, we extended our model and show an F-actin-dependent, leading-edge-specific immobilization of the Gβγ heterodimer, which is an important mediator of chemotactic responses. We show that this immobilization is due to activation of the chemotactic pathway and hypothesize that F-actin functions, either directly or indirectly, as a signaling-enhancing scaffold, suggesting a function for this mechanism in the stabilization of pseudopods and the onset of a persistent leading edge. Likewise, in terms of a balanced inactivation model (Levine et al., 2006), which suggests a possible inhibitory function for Gβγ, binding Gβγ to F-actin would prevent its inhibitory function specifically at the leading edge, finally leading to the steep amplification of the activation signal observed in experiments.

Materials and Methods

Cell culture and transformation

D. discoideum axenically growing strain Ax2 (Watts and Ashworth, 1970) was used in this study and referred to as wild type (wt), to discriminate from other genetic backgrounds that were used. The wt, *gβ*$^-$ (LW5), *gα2*$^-$ and *car1*$^-$ cells were transformed by electroporation with a plasmid, encoding the Gβ-YFP fusion protein. The same procedure was followed for wt and *gα2*$^-$ and *car1*$^-$ cells with the plasmid encoding the Gα2-YFP fusion protein. G418 (Geneticin, Invitrogen) was used to select for successfully transformed *D. discoideum*. Cells were grown as a monolayer on plastic dishes in axenic culture medium, HL5-C (Formedium), containing 100 μg/ml penicillin-streptomycin (1:1) (Invitrogen) and 20 μg/ml G418, at 22°C.

Cell preparation for measurements

To assess chemotactic competence, *D. discoideum* cells from axenic exponentially growing cultures were cultured in a plastic dish overnight in low fluorescence medium (Formedium). The physiological state of the cells treated in this way was comparable with cells starved for 1–2 hours. Next, the cells were detached from the plate, washed three times with developmental buffer (www.Dictybase.org), centrifuged for 3 minutes at 1500 r.p.m. and resuspended in 5 ml developmental buffer at a concentration of ~10^7 cells/ml in a 100 ml Erlenmeyer flask. After 1 hour of shaking at 150 r.p.m., the cells were pulsed with a peristaltic pump (Gilson, Minipulse 2) with 30 nM cAMP at 6-minute intervals, for 4 hours for the transformants in wt background and overnight for transformants in knockout backgrounds (*Dictyostelium discoideum* protocols, Eichiner Rivero, 2006; Humana Press). After pulsing, the cells were shaken for an additional 30 minutes, and finally diluted in developmental buffer to a concentration of 10^6 cells/ml. Cells were transferred into two-well chambered coverslips (1.5 Borosilicate Sterile, Lab Tek II) where they were allowed to adhere.

Developmental test

Gα2-YFP *gα2*$^-$ and Gβ-YFP *gβ*$^-$ transformants, as well as *gα2*$^-$ and *gβ*$^-$ cells were pulsed overnight with 30 nM cAMP as described later, were plated on non-nutrient 1.5% agar plates at a concentration of 3–4×10^7 cells/cm^2. After 24 hours, the developmental state was assessed.

Global cAMP stimulation assay

The developmental buffer, covering the developed cells in the chambered coverslips was supplemented with cAMP to a final concentration of 10 μM. Experiments were performed within 20 minutes of addition of cAMP.

Chemotaxis micropipette assay

Cells were placed at a distance of ~75 μm from the opening (r=0.25 μm) of a pipette (Eppendorf femtotip) filled with 10 μM cAMP. The internal pressure in the pipette was set to 40 kPa by means of a FemtoJet injector (Eppendorf). This set-up created a stable, shallow gradient estimated at 0.4 nM/μm cAMP over the cell body at a mid concentration of ~60 nM. The gradient caused polarization of the developed *D. discoideum* cells towards the micropipette tip. The region of interest was set to the leading and trailing edge (30% of the cell body) of a polarized cell, respectively.

Latrunculin A treatment

The developmental buffer, covering the developed cells in the chambered coverslips was supplemented with 0.5 μM latrunculin A. After 10 minutes, single-molecule measurements were performed for 10 minutes. To observe the effect of latrunculin A on the cell response to cAMP, 10 minutes after addition of the latrunculin A, cAMP was added to the buffer at final concentration of 10 μM, measurements were taken within 10 minutes of cAMP addition (Frigeri and Apgar, 1999).

Single-molecule microscopy

The experimental set-up for single-molecule imaging has been described in detail previously (Schmidt et al., 1996). The samples were mounted onto an inverted microscope (Axiovert100, Zeiss) equipped with a 100× objective (NA=1.4, Zeiss). The region of interest was set to 50×50 pixels. The apparent pixel size was 220 nm. Measurements were performed by illumination of the samples for 5 mseconds at 514 nm (Argon-ion laser, Spectra Physics) at intensity of 2 kW/cm^2. The cells were photobleached for a period of 2–5 seconds and sequences of 500 images with a time lag of 50 mseconds were taken. Use of an appropriate filter combination (Chroma) permitted the detection of the fluorescence signal on a liquid-nitrogen-cooled CCD camera (Princeton Instruments). The set-up allowed imaging of individual fluorophores at a signal-to-background-noise ratio of ~30, leading to a positional accuracy of σ_0=40 nm.

Estimation of the expression level of Gα2-YFP and Gβ-YFP

The expression level of Gα2-YFP in *gα2*$^-$, and Gβ-YFP in *gβ*$^-$ cells was calculated in the following manner. The image of a single fluorescent molecule was given by an intensity distribution characterized by a full-width-at-half-maximum of w_0=1.7, pixel=0.37 μm. The average signal for a single YFP molecule was S_1=220 counts when illuminated with 2 kW/cm^2 for 5 mseconds at 514 nm (Harms et al., 2001). The fluorescence of Gβ-YFP at the apical membrane at identical conditions was $S_{G\beta}$=4300 counts/pixel, and for Gα2-YFP $S_{G\alpha2}$=4000 counts/pixel. The surface of the membrane for a whole cell (approximated by a spheroid with a short axis of r_1=5 μm and long axis r_2=10 μm) is about 540 μm^2. The fluorescence data were used in the estimation of the expression level yielding $(S_{G\beta}/S_1)\times(A/w_0^2)$=7.7×$10^4$ Gβ-YFP and 7.2×10^4 Gα2-YFP molecules per cell. A similar estimation has been done for the receptor yielding 4×10^4 cAR1 molecules per cell (de Keijzer et al., 2008).

Particle image correlation spectroscopy (PICS)

The reconstruction of trajectories from molecule positions is severely hampered by blinking and photobleaching of eYFP (Harms et al., 2001). Therefore, we used an alternative analysis method, particle image correlation spectroscopy (PICS), which is described in detail elsewhere (Semrau and Schmidt, 2007). In short, the cross-correlation between single-molecule positions at two different time lags is calculated. Subsequently, the linear contribution from uncorrelated molecules in close proximity is subtracted. This results in the cumulative distribution function $cdf(r^2,t_{lag})$, which yields the distribution of squared jump widths within the given time lag t_{lag}. For each time lag $cdf(r^2,t_{lag})$ is fitted to a two-fraction model Eq. 4 (Fig. 1C,D).

Analysis of the cumulative probability functions

From the jump-width distributions, the diffusion characteristics of all molecules is extracted. Given that the population of particles is homogeneous, the diffusion equation is solved for $cdf(r^2,t_{lag})$ given by:

$$cdf(r^2,t_{lag}) = 1-\exp\left(\frac{-r^2}{MSD(t_{lag})}\right), \quad (3)$$

where MSD(t_{lag}) is the mean-square displacement at time lag t_{lag}. Given the exponential distribution in r^2, data are represented on log(r^2)-scale. Our experimental data could not be fitted with this one fraction model, however (Fig. 1D). Therefore the data were fit to a two-fraction model described by:

$$cdf(r^2,t_{lag}) = 1-\alpha\exp\left(\frac{-r^2}{MSD_2(t_{lag})}\right)-(1-\alpha)\exp\left(\frac{-r^2}{MSD_1(t_{lag})}\right), \quad (4)$$

where $MSD_2(t_{lag})$ is the characteristic mean squared displacement for the slow fraction of size α, and $MSD_1(t_{lag})$ the characteristic mean squared displacement for the fast fraction of size 1–α. The bi-exponential fit properly describes the experimental results (Fig. 1D). This showed that there are two fractions of Gβ-YFP and of Gα2-YFP molecules that differ in their mobility on the membrane. Molecules were defined immobile when their MSD for the largest time lag (0.4 second) was smaller than twice the positional accuracy. Together with Eq. 1, this leads to an upper estimate for their diffusion constant of $D_{immobile}$<0.001 μm^2/second.

We would like to thank the Dicty Stock Center (http://dictybase.org/StockCenter/StockCenter.html) for generously providing the *Dictyostelium discoideum* strains and plasmids. Sandra de Keijzer (U. Nijmegen, The Netherlands) is thanked for helpful discussions. This work was supported by funds from the Human Frontiers Science Program grant RGP66/2004, and the Dutch CYTTRON consortium sponsored by the ministry of economic affairs.

Supplementary material available online at
http://jcs.biologists.org/cgi/content/full/123/17/2922/DC1

References

Chen, L., Janetopoulos, C., Huang, Y. E., Iijima, M., Borleis, J. and Devreotes, P. N. (2003). Two phases of actin polymerization display different dependencies on PI(3,4,5)P3 accumulation and have unique roles during chemotaxis. *Mol. Biol. Cell* **14**, 5028-5037.

Chen, L., Iijima, M., Tang, M., Landree, M. A., Huang, Y. E., Xiong, Y., Iglesias, P. A. and Devreotes, P. N. (2007). PLA2 and PI3K/PTEN pathways act in parallel to mediate chemotaxis. *Dev. Cell* **12**, 603-614.

Comer, F. I. and Parent, C. A. (2002). PI 3-kinases and PTEN: how opposites chemoattract. *Cell* **109**, 541-544.

de Keijzer, S., Serge, A., van Hemert, F., Lommerse, P. H. M., Lamers, G. E. M., Spaink, H. P., Schmidt, T. and Snaar-Jagalska, B. E. (2008). A spatially restricted increase in receptor mobility is involved in directional sensing during Dictyostelium discoideum chemotaxis. *J. Cell Sci.* **121**, 1750-1757.

Devreotes, P. N. and Steck, T. L. (1979). Cyclic 3′,5′ AMP relay in Dictyostelium discoideum. II. Requirements for the initiation and termination of the response. *J. Cell Biol.* **80**, 300-309.

Eichinger, L. and Rivero, F. (2006) *Dictiostelium Discoideum Protocols*: In *Methods in Molecular Biology*, Berlin, Springer.

Elzie, C. A., Colby, J., Sammons, M. A. and Janetopoulos, C. (2009). Dynamic localization of G proteins in Dictyostelium discoideum. *J. Cell Sci.* **122**, 2597-2603.

Fischer, T., Lu, L., Haigler, H. T. and Langen, R. (2007). Annexin B12 is a sensor of membrane curvature and undergoes major curvature-dependent structural changes. *J. Biol. Chem.* **282**, 9996-10004.

Franca-Koh, J., Kamimura, Y. and Devreotes, P. N. (2006). Navigating signaling networks: chemotaxis in Dictyostelium discoideum. *Curr. Opin. Genet. Dev.* **16**, 333-338.

Frigeri, L. and Apgar, J. R. (1999). The role of actin microfilaments in the down-regulation of the degranulation response in RBL-2H3 mast cells. *J. Immunol.* **162**, 2243-2250.

Funamoto, S., Meili, R., Lee, S., Parry, L. and Firtel, R. A. (2002). Spatial and temporal regulation of 3-phosphoinositides by PI 3-kinase and PTEN mediates chemotaxis. *Cell* **109**, 611-623.

Harms, G. S., Cognet, L., Lommerse, P. H., Blab, G. A. and Schmidt, T. (2001). Autofluorescent proteins in single-molecule research: applications to live cell imaging microscopy. *Biophys. J.* **80**, 2396-2408.

Iijima, M. and Devreotes, P. N. (2002). Tumor suppressor PTEN mediates sensing of chemoattractant gradients. *Cell* **109**, 599-610.

Jaakola, V. P., Griffith, M. T., Hanson, M. A., Cherezov, V., Chien, E. Y. T., Lane, J. R., IJzerman, A. P. and Stevens, R. C. (2008). The 2.6 Angstrom crystal structure of a human A2A adenosine receptor bound to an antagonist. *Science* **322**, 1211-1217.

Janetopoulos, C., Jin, T. and Devreotes, P. N. (2001). Receptor-mediated activation of heterotrimeric G-proteins in living cells. *Science* **291**, 2408-2411.

Janssens, P. M. and Van Haastert, P. J. (1987). Molecular basis of transmembrane signal transduction in Dictyostelium discoideum. *Microbiol. Rev.* **51**, 396-418.

Jin, T., Zhang, N., Long, Y., Parent, C. A. and Devreotes, P. N. (2000). Localization of the G protein complex in living cells during chemotaxis. *Science* **287**, 1034-1036.

Kamimura, Y., Xiong, Y., Iglesias, P. A., Hoeller, O., Bolourani, P. and Devreotes, P. N. (2008). PIP3-independent activation of TorC2 and PKB at the cell's leading edge mediates chemotaxis. *Curr. Biol.* **18**, 1034-1043.

Kimmel, A. R. and Parent, C. A. (2003). The signal to move: D. discoideum go orienteering. *Science* **300**, 1525-1527.

Kusumi, A., Sako, Y. and Yamamoto, M. (1993). Confined lateral diffusion of membrane receptors as studied by single particle tracking (nanovid microscopy). Effects of calcium-induced differentiation in cultured epithelial cells. *Biophys. J.* **65**, 2021-2040.

Levine, H., Kessler, D. A. and Rappel, W. J. (2006). Directional sensing in eukaryotic chemotaxis: a balanced inactivation model. *Proc. Natl. Acad. Sci. USA* **103**, 9761-9766.

Lilly, P., Wu, L., Welker, D. L. and Devreotes, P. N. (1993). A G-protein beta-subunit is essential for Dictyostelium development. *Genes Dev.* **7**, 986-995.

Nobles, M., Benians, A. and Tinker, A. (2005). Heterotrimeric G proteins precouple with G protein-coupled receptors in living cells. *Proc. Natl. Acad. Sci. USA* **102**, 18706-18711.

Palczewski, K., Kumasaka, T., Hori, T., Behnke, C. A., Motoshima, H., Fox, B. A., Trong, I. L., Teller, D. C., Okada, T., Stenkamp, R. E. et al. (2000). Crystal structure of rhodopsin: a G protein-coupled receptor. *Science* **289**, 739-745.

Parent, C. A., Blacklock, B. J., Froehlich, W. M., Murphy, D. B. and Devreotes, P. N. (1998). G protein signaling events are activated at the leading edge of chemotactic cells. *Cell* **95**, 81-91.

Pawson, T. and Scott, J. D. (1997). Signaling through scaffold, anchoring, and adaptor proteins. *Science* **278**, 2075-2080.

Potma, E. O., de Boeij, W. P., Bosgraaf, L., Roelofs, J., Van Haastert, P. J. and Wiersma, D. A. (2001). Reduced protein diffusion rate by cytoskeleton in vegetative and polarized dictyostelium cells. *Biophys. J.* **81**, 2010-2019.

Rasmussen, S. G. F., Choi, H. J., Rosenbaum, D. M., Kobilka, T. S., Thian, F. S., Edwards, P. C., Burghammer, M., Ratnala, V. R. P., Sanishvili, R., Fischetti, R. F. et al. (2007). Crystal structure of the human [bgr]2 adrenergic G-protein-coupled receptor. *Nature* **450**, 383-387.

Schmidt, T., Schutz, G. J., Baumgartner, W., Gruber, H. J. and Schindler, H. (1996). Imaging of single molecule diffusion. *Proc. Natl. Acad. Sci. USA* **93**, 2926-2929.

Semrau, S. and Schmidt, T. (2007). Particle image correlation spectroscopy (PICS): retrieving nanometer-scale correlations from high-density single-molecule position data. *Biophys. J.* **92**, 613-621.

Ueda, M., Sako, Y., Tanaka, T., Devreotes, P. N.. and Yanagida, T. (2001). Single-molecule analysis of chemotactic signaling in Dictyostelium cells. *Science* **294**, 864-867.

van Haastert, P. J., Bishop, J. D. and Gomer, R. H. (1996). The cell density factor CMF regulates the chemoattractant receptor cAR1 in Dictyostelium. *J. Cell Biol.* **134**, 1543-1549.

Veltman, D. M., Van Haastert, P. J. (2006). Guanylyl cyclase protein and cGMP product independently control front and back of chemotaxing *Dictyostelium* cells. *Mol. Biol. Cell.* 17, 3921-3929.

Veltman, D. M. and Van Haastert, P. J. (2008). Four key signaling pathways mediating chemotaxis in *Dictyostelium discoideum*. *J. Cell Biol.* **180**, 747-753.

Watts, D. J. and Ashworth, J. M. (1970). Growth of myxameobae of the cellular slime mould Dictyostelium discoideum in axenic culture. *Biochem. J.* **119**, 171-174.

Weisswange, I., Bretschneider, T. and Anderson, K. I. (2005). The leading edge is a lipid diffusion barrier. *J. Cell Sci.* **118**, 4375-4380.

Wessels, D., Schroeder, N. A., Voss, E., Hall, A. L., Condeelis, J. and Soll, D. R. (1989). cAMP-mediated inhibition of intracellular particle movement and actin reorganization in Dictyostelium. *J. Cell Biol.* **109**, 2841-2851.

Wettschureck, N. and Offermanns, S. (2005). Mammalian G proteins and their cell type specific functions. *Physiol. Rev.* **85**, 1159-1204.

Xu, X., Meier-Schellersheim, M., Jiao, X., Nelson, L. E. and Jin, T. (2005). Quantitative imaging of single live cells reveals spatiotemporal dynamics of multistep signaling events of chemoattractant gradient sensing in Dictyostelium. *Mol. Biol. Cell* **16**, 676-688.

Zhang, N., Long, Y. and Devreotes, P. N. (2001). Ggamma in Dictyostelium: its role in localization of Gbeta gamma to the membrane is required for chemotaxis in shallow gradients. *Mol. Biol. Cell* **12**, 3204-3213.